Synthesis and Monitoring of α-$Bi_2Mo_3O_{12}$ Catalyst Formation using Thermo-Raman Spectroscopy

Anil Ghule,[a] Shin-Hwa Tzing,[a] Jia-Yaw Chang,[a] Kalyani Ghule,[a] Hua Chang,[a] and Yong Chien Ling*[a]

Keywords: Thermo-Raman spectroscopy / Thermochemistry / Dehydration / Phase transformations / Bismuth / α-$Bi_2Mo_3O_{12}$ catalyst

Thermo-Raman spectroscopy was used to monitor the dehydration and phase transformations of $Bi_2Mo_3O_{12}\cdot 5H_2O$. The hydrated forms $Bi_2Mo_3O_{12}\cdot 5H_2O$, $Bi_2Mo_3O_{12}\cdot 4.75H_2O$, $Bi_2Mo_3O_{12}\cdot 3H_2O$, $Bi_2Mo_3O_{12}\cdot 2H_2O$, and anhydrous $Bi_2Mo_3O_{12}$ were observed during dehydration in the wavelength range from 200 to 1400 cm^{-1}. Representative Raman spectra of these compounds are reported for the first time. The thermo-Raman intensity thermogram showed a systematic dehydration in four steps, and the differential thermo-Raman intensity thermogram confirmed this. Thermogravimetry, differential thermogravimetry, and differential scanning calorimetry results were in harmony with the results of the thermo-Raman spectroscopy. Additionally, the dehydration resulting in formation of anhydrous $Bi_2Mo_3O_{12}$ (amorphous $Bi_2Mo_3O_{12}$ phase) and the final transformation into the α-$Bi_2Mo_3O_{12}$ phase was observed to be a dynamic thermal process. The slow, controlled heating rate produced α-$Bi_2Mo_3O_{12}$ catalyst with a particle size averaging 200 nm. The catalyst formed was further characterized by Fourier transform infrared spectroscopy, X-ray diffraction, time of flight SIMS, transmission electron microscopy, and energy-dispersive X-ray analysis.

Introduction

Bismuth molybdates (α-$Bi_2Mo_3O_{12}$, β-$Bi_2Mo_2O_9$, and γ-Bi_2MoO_6 phases) are very popular and widely studied catalysts because of their commercial importance.[1] Extensive investigation of their ability to catalyze the selective oxidation and ammoxidation of alkenes[1−4] and hydrogen sulfide[5] has been carried out. The importance of bismuth molybdates is not limited to catalysis since they also show interesting physical properties with potential technological applications. Vannier et al.[6] reported $Bi_{26}Mo_{10}O_{69}$ as being the first unidimensional bismuth-based oxide ion conductor. Bismuth molybdates also show good optical quality with a wide transmission window between 0.415 and 5.2 μm.[7] Additionally, single crystals with large photon-phonon scattering cross-sections have attracted increasing interest as acousto-optical materials. They possess low optic and acoustic absorptions, good mechanical properties, and chemical stability (e.g. insolubility in water).[8,9] The tetragonal phases of thin-film bismuth-derived compounds are efficient photoconductors[10] and thin films of bismuth molybdates are effective gas sensors showing potential applications in breathalyzer devices.[11]

Bismuth molybdate catalyst systems have been structurally characterized,[12] and studied extensively by different techniques such as X-ray absorption,[13] X-ray diffraction,[14] neutron diffraction,[15] time-of-flight SIMS,[16] electron diffraction techniques,[17] high-resolution electron microscopy and vibrational spectroscopy.[18−20] Raman spectroscopy has proved to be an effective tool for the characterization of the structures of transition metal oxides in the bulk and two-dimensional surface phases.[21] Thus, a systematic study has been made of Raman stretching frequency, bond length, and bond strength empirical correlations. However, all these studies concentrated on the α-$Bi_2Mo_3O_{12}$ phase and little attention has been paid to $Bi_2Mo_3O_{12}\cdot 5H_2O$ and the other hydrated species, which could be important in optics and acoustic applications. The catalytic α-$Bi_2Mo_3O_{12}$ phase used in earlier studies was usually prepared by co-precipitation,[22] sol-gel methods,[23] solid-state reactions,[20] spray drying,[24] high-temperature calcination of solid mixtures or several other methods.[25] However, co-precipitation techniques result in co-precipitation of pure hydroxides and also precipitate bismuth with polymerized Mo ions. Solid-state reactions yield byproducts (phases) formed as a result of non-stoichiometric compositions,[26] and thus require several high-temperature calcination steps and regrinding to give a single, selective phase of the catalyst. Attempts to use mechanical mixtures have been made because of co-operative catalytic effects in multiphase systems where individual catalytic phases were prepared separately before mixing. Occasionally, pure forms, often contaminated with small amounts (ca. 2%) of other phases, have been reported.[27] Thus, monitoring of the

[a] Department of Chemistry, National Tsing Hua University, Hsinchu, Taiwan 30043, Republic of China
Fax: (internat.) + 886-35711082
E-mail: ycling@mx.nthu.edu.tw

preparation process is important to obtain selectively a single phase. This should enable a clarification of the roles and stabilities of individual bismuth molybdate phases during selective oxidations.

Thermogravimetry (TG), differential thermal analysis (DTA), and differential scanning calorimetry (DSC) are techniques generally used to study the thermal properties of solid samples in dynamic and static thermal processes.[28] However, these techniques fail to provide direct information about the phases and their compositions during a dynamic process. Thermo-Raman spectroscopy (TRS) is a useful technique in which successive collection of Raman spectra yields many details about a dynamic thermal process. The compositional changes of all the intermediates and phase transformations can be easily monitored and identified on a time scale of seconds and in temperature increments of one degree. The Raman intensity and the derivative of the Raman intensity of the characteristic band are plotted as a function of temperature and are the thermo-Raman intensity (TRI) and differential thermo-Raman intensity (DTRI) thermograms, respectively. These provide detailed quantitative information about the compositional changes and phase transformations[29] and can be compared with thermograms from TG, DTA, and DSC. Thus, thermo-Raman spectroscopy should be an ideal technique for monitoring and study of the morphological and compositional changes occurring during heating and calcinations.

In this work, the compositional variations of $Bi_2Mo_3O_{12}\cdot 5H_2O$ were observed by thermo-Raman spectroscopy in the temperature range from 25 to 600 °C. Spectral variation monitored in the H_2O and MoO_4^{2-} regions revealed four dehydrations resulting in formation of $Bi_2Mo_3O_{12}\cdot 4.75H_2O$, $Bi_2Mo_3O_{12}\cdot 3H_2O$, $Bi_2Mo_3O_{12}\cdot 2H_2O$, and $Bi_2Mo_3O_{12}$, respectively. Characteristic Raman spectra representing all the intermediates were obtained. The TRI thermogram and DTRI thermogram for the H_2O bands were plotted revealing four steps of dehydration with a proportionate loss of water in each step. The TG thermogram showed loss of 9% weight for the entire dehydration process suggesting loss of five H_2O molecules, with differential thermogravimetry (DTG) thermograms showing dips at 95, 148, 190, and 221 °C. Formation of anhydrous $Bi_2Mo_3O_{12}$ (amorphous $Bi_2Mo_3O_{12}$) in the temperature range from 290 to 320 °C was followed by transformation to the α-$Bi_2Mo_3O_{12}$ phase, which was identified by its Raman spectrum in the temperature range from 320 to 345 °C. This resulting α-$Bi_2Mo_3O_{12}$ phase was subjected to morphological and phase purity characterization.

Results and Discussion

Thermograms

The TG thermogram of $Bi_2Mo_3O_{12}\cdot 5H_2O$ in the temperature range from 25 to 600 °C is shown in Figure 1(a). It indicates a weight loss of 9% for the entire dehydration process suggesting the loss of five water molecules (calculated weight loss for five water molecules = 9.1%). The TG thermogram shows weight losses of 0.5% or 0.25 water molecules (T = 90−100 °C to form $Bi_2Mo_3O_{12}\cdot 4.75H_2O$), 3.5% or 1.9 water molecules (T = 100−165 °C to form $Bi_2Mo_3O_{12}\cdot 3H_2O$), 5.4% or 2.93 molecules (T = 165−200 °C to form $Bi_2Mo_3O_{12}\cdot 2H_2O$), and 9% or 4.94 water molecules (T = 200−290 °C to form anhydrous $Bi_2Mo_3O_{12}$) in the first, second, third, and fourth steps of dehydration, respectively. The entire dehydration process extended up to 290 °C. The observed weight losses were in close agreement with the theoretical weight losses of 0.5, 3.6, 5.4, and 9.1%, in the respective dehydration steps. Further heating gave a slight loss in weight upon transformation into the α-$Bi_2Mo_3O_{12}$ phase. This might be due to the diffusion of lattice oxygen atoms to the surface and its subsequent loss, as the bulk is known to act as an oxygen carrier.[1]

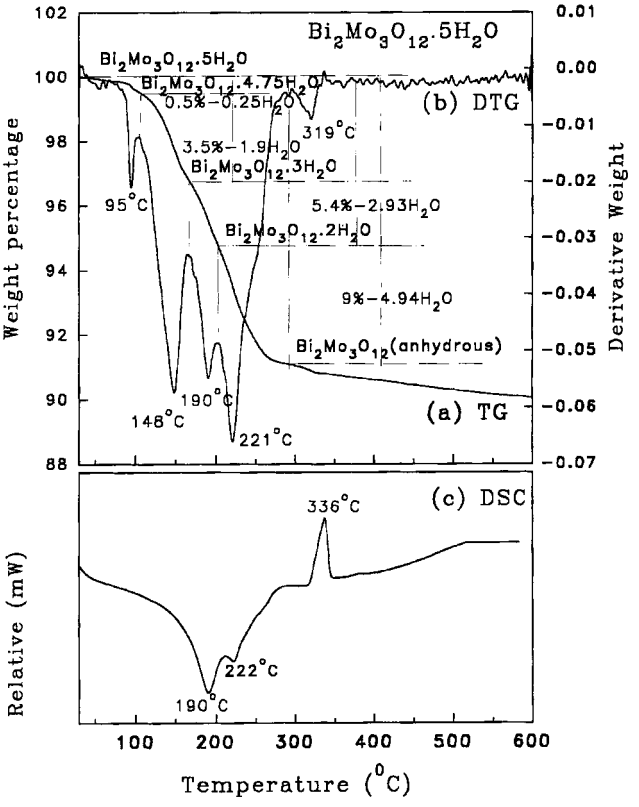

Figure 1. (a) TG, (b) DTG, and (c) DSC thermograms from 25 to 600 °C starting from $Bi_2Mo_3O_{12}\cdot 5H_2O$

The DTG thermogram, which is the derivative of the TG thermogram, is shown in Figure 1(b). It shows dips at 95, 148, 190, and 221 °C indicating maximum weight losses during the first, second, third, and fourth dehydration steps, respectively. A slight shoulder at 250 °C to the dip at 221 °C is due to the prolonged fourth step of dehydration. The dip at 319 °C is assigned to the transformation from the anhydrous form to the α-$Bi_2Mo_3O_{12}$ phase. No further information could be extracted at higher temperatures.

There are several reports about the presence of the hydrated species. Murakami and Imai[30] reported the presence of $Bi_2Mo_3O_{12}\cdot 4.75H_2O$ and anhydrous $Bi_2Mo_3O_{12}$ (amorphous) based on thermogravimetric (TG) analysis.

The amorphous phase formation occurred at 150 °C based on the X-ray diffraction pattern, contradicting their TGA data, which indicated a transition at 250 °C. Yinjie and Aimin[31] estimated the presence of $Bi_2Mo_3O_{12}\cdot 3.86H_2O$ based on their TGA data. Thus, it was of interest to determine the different hydrated species of $Bi_2Mo_3O_{12}\cdot 5H_2O$.

The DSC thermogram of $Bi_2Mo_3O_{12}\cdot 5H_2O$ in the temperature range from 25 to 600 °C is shown in Figure 1(c). It has a broad endotherm at 190 °C accounting for the first three dehydration steps and an endotherm at 222 °C for the fourth dehydration step . The sharp exotherm at 336 °C (enthalpy = −22.6 J/g) is as a result of the phase transformation from the amorphous phase to the α-$Bi_2Mo_3O_{12}$ phase. The DSC thermogram also shows that the entire dehydration process extends up to 290 °C, in contrast to the earlier report by Murakami and Imai.[30]

Thermo-Raman Studies

Extensive theoretical considerations and experimental studies have shown that vibrational spectroscopy of powdered samples provides information not only about the phases, but also about the size, shape, and state of aggregation of the particles that constitute the powder.[32] Assuming the internal and external modes of the sample to be independent of one another, the internal modes of metal oxide molecules within the unit cell of a crystal occur in the medium- and high-frequency regions (> 400 cm^{-1} for the MoO_4^{2-} species). External modes, including translational and librational modes, occur at lower frequencies (< 400 cm^{-1}). This helps in identification and assignment of species based on their characteristic Raman spectra. The internal modes in the range from 400 to 1200 cm^{-1} provide information about the environment around the MoO_4^{2-} ions. The free molybdate ion, MoO_4^{2-}, is tetrahedral with point group T_d symmetry. It has four vibrational modes $\nu_1(A_1)$, $\nu_2(E)$, $\nu_3(T_2)$, and $\nu_4(T_2)$. The stretching modes connect $\nu_1(A_1)$ and $\nu_3(T_2)$, while the bending modes connect $\nu_2(E)$ and $\nu_4(T_2)$. In addition, the α-$Bi_2Mo_3O_{12}$ phase contains three different tetrahedra which might result in different band positions. Matsuura et al.[18] reported six bands around 900 and 800 cm^{-1} attributed to the stretching modes of each tetrahedral species. Theobald et al.,[15] in their XANES experiments, observed that the Mo^{6+} ions in

Table 1. Raman bands for $Bi_2Mo_3O_{12}\cdot 5H_2O$, $Bi_2Mo_3O_{12}\cdot 4.75H_2O$, $Bi_2Mo_3O_{12}\cdot 3H_2O$ $Bi_2Mo_3O_{12}\cdot 2H_2O$, anhydrous $Bi_2Mo_3O_{12}$, and α-$Bi_2Mo_3O_{12}$

$Bi_2Mo_3O_{12}$ $5H_2O$ 25 °C	$Bi_2Mo_3O_{12}$ $4.75H_2O$ 100 °C	$Bi_2Mo_3O_{12}$ $3H_2O$ 165 °C	$Bi_2Mo_3O_{12}$ $2H_2O$ 200 °C	$Bi_2Mo_3O_{12}$ (anhydrous) 290 °C	α-$Bi_2Mo_3O_{12}$ 450 °C	Assignment[a]
		3549 w[b]	3542 w			
		3502 w	3502 w	3521 w		
3453 s	3451 s	3462 s	3458 w			
		3305 w				H_2O
3265 m	3285 w	3273 w				(stre.vib.)
		3233 w	3220 w	3220 w		
					996 s	
					959 w	
920 s	920 s	920 s	920 s	928 m		
				905 m	899 s	Mo−O
866 s	866 s	866 s	864 s			stre.vib.
				844 w		
			820 w		824 s	
684 w	684 w	684 w		681 w	669 s	
649 s	649 s	649 s	657 m			
525 s	525 s	525 s	525 m			
					542 w	Bi−O stre.
499 w	499 w	501 w			504 m	vib.
					495 w	Mo_2O_2 dioxo
467 w	467 w	467 w				
418 s	418 s	418 s	420 m			
374 s	374 s	374 s	374 m	374 w	370 s	
352 w	352 m	352 w				Mo−O
342 w		342 w	342 w		340 w	bend./wag.
324 w	322 w	322 w			324 w	and external
292 w	289 w	291 w			289 s	vib. modes
267 w	267 w	267 w				

[a] Refs.[12,21] [b] s = strong, m = medium, w = weak, and stre. vib. = stretching vibrations.

α-$Bi_2Mo_3O_{12}$ are surrounded by five oxygen atoms in an asymmetric Mo−O_5 coordination environment, with an average Mo−O interatomic distance of 1.91 Å. However, the Fourier transform EXAFS data revealed a substantial structural complexity. The irregular oxygen coordination about the Mo^{6+} ions results in three peaks at 1.26, 1.53, and 1.97Å. The more distant Bi and Mo cations around this molybdenum give rise to three peaks at 2.86, 3.30, and 3.65 Å, which are due to Mo···Mo, Mo···Bi, and Mo···Mo/Bi back scatterings, respectively.[13] Generally, in dynamic thermal process within crystals, structural distortions may occur, which lower the symmetry causing shifting and splitting of the bands. Raman bands for $Bi_2Mo_3O_{12}$ fall between 200 and 1200 cm^{-1} and are assigned as in Table 1. The broad band in the range from 3200 to 3600 cm^{-1} is due to lattice H_2O (antisymmetric and symmetric OH stretching).[21]

Dehydration

First Dehydration

Figure 2(A)(a) shows the characteristic Raman spectrum of $Bi_2Mo_3O_{12}·5H_2O$ at 25 °C in the H_2O region from 3000 to 3700 cm^{-1}. The two broad bands at 3453 and 3265 cm^{-1} at 25 °C represent the lattice H_2O. As the temperature rises above 60 °C, these bands shift to 3451 and 3285 cm^{-1}, respectively, as $Bi_2Mo_3O_{12}·4.75H_2O$ forms during the first dehydration step. The characteristic Raman spectrum of $Bi_2Mo_3O_{12}·4.75H_2O$ in the water region is shown in Figure 2(A)(b) (100 °C). The actual transformation occurs in the temperature range from 60 to 75 °C, where the weakly bound water molecule (water of crystallization) is easily lost.

The corresponding characteristic Raman spectrum of $Bi_2Mo_3O_{12}·5H_2O$ at 25 °C in the MoO_4^{2-} region (from 200 to 1200 cm^{-1}) is shown in Figure 2(B)(a). A slight decrease in intensity of the two bands at 920 and 866 cm^{-1} is observed with the rise in temperature to 100 °C. The bands at 684, 649, 525, 499, 467, 418, 374, 352, 342, 292, and 267 cm^{-1} show a slight broadening. No distinct changes in spectrum and symmetry of MoO_4^{2-} were observed since only a small amount of water is lost in this step. Among the noticeable changes, the weak band at 499 cm^{-1} appears as a shoulder to the band at 525 cm^{-1} and the doublet at 352 and 342 cm^{-1} disappears as the temperature rises above 60 °C. These spectral changes were especially evident in the temperature range from 60 to 75 °C and are represented in the characteristic spectrum of $Bi_2Mo_3O_{12}·4.75H_2O$ shown in Figure 2(B)(b). The first dehydration is the transformation from $Bi_2Mo_3O_{12}·5H_2O$ to $Bi_2Mo_3O_{12}·4.75H_2O$. To the best of our knowledge, no crystal data are available for $Bi_2Mo_3O_{12}·5H_2O$. However, the structure of $Bi_2Mo_3O_{12}·5H_2O$ could be similar to that of $Bi_2Mo_3O_{12}·4.75H_2O$ (reported by Murakami and Imai,[30]) based on the similarity of their Raman spectra. The crystal structure of $Bi_2Mo_3O_{12}·4.75H_2O$ has a monoclinic unit cell, with lattice parameters calculated to be a = 6.334, b = 11.593, c = 5.777 Å and β = 113.166° as indexed from the X-ray diffraction pattern.

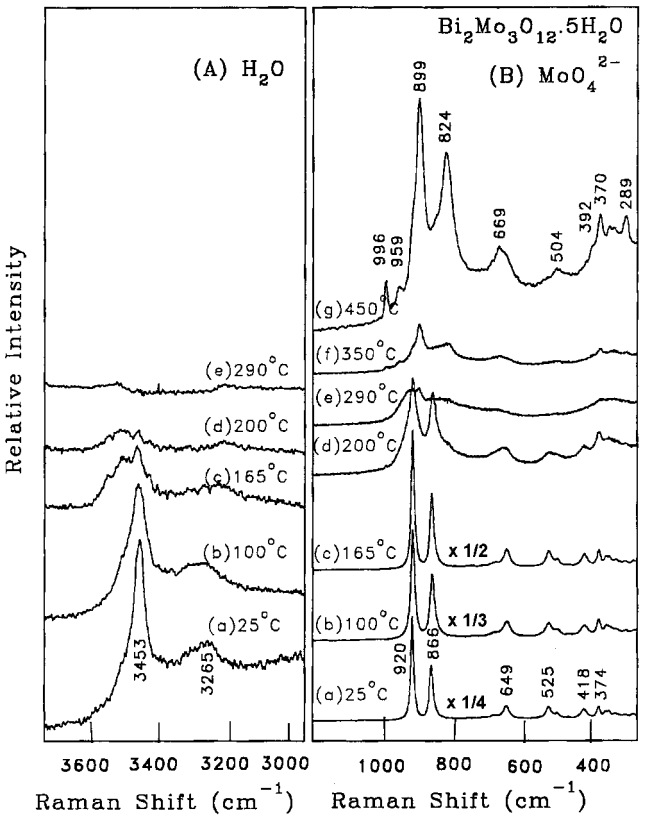

Figure 2. Characteristic thermo-Raman spectra of $Bi_2Mo_3O_{12}·5H_2O$ during the dehydration and of the intermediate hydrated species observed: (a) $Bi_2Mo_3O_{12}·5H_2O$ (25 °C; intensity reduced 4 times); (b) $Bi_2Mo_3O_{12}·4.75H_2O$ (100 °C; intensity reduced 3 times); (c) $Bi_2Mo_3O_{12}·3H_2O$ (165 °C; intensity reduced 2 times); (d) $Bi_2Mo_3O_{12}·2H_2O$ (200 °C); (e) $Bi_2Mo_3O_{12}$ (290 °C); (f) $Bi_2Mo_3O_{12}$ amorphous phase (350 °C); (g) α-$Bi_2Mo_3O_{12}$ (450 °C) in (A) the H_2O region from 3000 to 3700 cm^{-1} and (B) the MoO_4^{2-} region from 200 to 1200 cm^{-1}

Second Dehydration

The spectral variations in the H_2O region for the second dehydration in the temperature range from 100 to 165 °C were observed and the characteristic Raman spectrum of $Bi_2Mo_3O_{12}·3H_2O$ is shown in Figure 2(A)(c). The broad band at 3451 cm^{-1} further broadens and shifts to 3462 cm^{-1} as the temperature rises above 128 °C. Two broad bands at 3549 and 3502 cm^{-1} emerge and become distinct with the rise in temperature to 165 °C. The broad band at 3285 cm^{-1}splits into bands at 3305, 3273, and 3233 cm^{-1}. Overall, a decrease in intensity of the H_2O bands was observed with major spectral changes in the temperature range from 128 to 132 °C.

Similar changes were observed in the MoO_4^{2-} region for the second dehydration in the temperature range from 100 to 165 °C, and the characteristic Raman spectrum of $Bi_2Mo_3O_{12}·3H_2O$ is shown in Figure 2(B)(c). The bands observed at 920 and 866 cm^{-1} show a notable decrease in intensity as the temperature rises to 165 °C. The singlet at 351 cm^{-1}, observed at 100 °C, splits into two bands at 352 and 342 cm^{-1} as the temperature rises above 128 °C. The

band at 322 cm^{-1} becomes distinct and the bands at 289 and 263 cm^{-1} shift to 291 and 267 cm^{-1}, respectively. The spectral changes in the temperature range from 128 to 132 °C correspond to a second dehydration to form $Bi_2Mo_3O_{12}·3H_2O$ from $Bi_2Mo_3O_{12}·4.75H_2O$. The two water molecules lost below 165 °C are attributed to the water of crystallization. To the best of our knowledge, the Raman spectrum of $Bi_2Mo_3O_{12}·3H_2O$ is reported here for the first time and crystal structure data for $Bi_2Mo_3O_{12}·3H_2O$ are yet to be reported. However, based on the similarity of their Raman spectra, its structure is expected to be similar to $Bi_2Mo_3O_{12}·4.75H_2O$ with a slight variation in lattice parameters. Yinjie and Aimin,[31] reported the crystal structure of $Bi_2Mo_3O_{12}·3.86H_2O$ as monoclinic, with lattice parameters calculated to be a = 6.338, b = 11.658, c = 5.787 Å and β = 113.168° as indexed from the X-ray diffraction pattern.

Third Dehydration

Spectral variations were observed in the H_2O region for the third dehydration in the temperature range from 165 to 200 °C with a transformation temperature at 192 °C. The characteristic Raman spectrum of $Bi_2Mo_3O_{12}·2H_2O$ obtained after the third dehydration is shown in Figure 2(A)(d). The spectrum at 165 °C shows broad bands at 3549 and 3462 cm^{-1}. These bands gradually shift to 3542 and 3458 cm^{-1}, respectively, with the rise in temperature above 190 °C. The band at 3502 cm^{-1} further broadens and the weak bands at 3305 and 3273 cm^{-1} disappear as the temperature approaches 200 °C. The weak band at 3233 cm^{-1} shifts to 3220 cm^{-1}.

Spectral variations were also observed in the MoO_4^{2-} region for the third dehydration step in the temperature range from 165 to 200 °C and the characteristic spectrum of $Bi_2Mo_3O_{12}·2H_2O$ is shown in Figure 2(B)(d). The band at 920 cm^{-1} broadens and drastically decreases in intensity. A shoulder at 820 cm^{-1} to the band at 864 cm^{-1} starts appearing at 193 °C and gradually resolves as the temperature rises to 200 °C. The band at 649 cm^{-1} broadens and shifts to 657 cm^{-1} and the shoulder at 684 cm^{-1} gradually disappears as the temperature rises to 200 °C. Similarly, the band at 525 cm^{-1} becomes weak and the shoulder at 501 cm^{-1} and the weak band at 467 cm^{-1} disappear. The doublet at 352 and 342 cm^{-1} merges to form a broad singlet at 342 cm^{-1}. The lower modes at 322, 291, and 267 cm^{-1} also disappear as the temperature rises to 200 °C. The major changes observed in the spectra indicate the drastic change in symmetry of MoO_4^{2-}, even though only one water molecule is lost in this step, resulting in the transformation from $Bi_2Mo_3O_{12}·3H_2O$ to $Bi_2Mo_3O_{12}·2H_2O$. This shows that the water molecule evolved in this third dehydration must be different from the two water molecules evolved in the previous dehydrations and that it is associated directly with the structural composition. It is assigned as a water of constitution. The crystal structure of $Bi_2Mo_3O_{12}·2H_2O$ is yet to be reported.

Fourth Dehydration

The spectral variations in the H_2O region for the fourth dehydration in the temperature range from 200 to 290 °C were monitored and the characteristic Raman spectrum for anhydrous $Bi_2Mo_3O_{12}$ is shown in Figure 2(A)(e). The weak, broad bands observed at 3542, 3502, 3458, and 3220 cm^{-1} gradually disappear when the temperature reaches 290 °C. This indicates a complete loss of water to form anhydrous $Bi_2Mo_3O_{12}$. The Raman spectral profile appears almost flat.

Similarly, spectral changes were clearly observed in the MoO_4^{2-} region for the fourth dehydration in the temperature range from 200 to 290 °C with a transformation temperature observed at 220 °C. The characteristic Raman spectra of the anhydrous $Bi_2Mo_3O_{12}$ is shown in Figure 2(B)(e). The broad band at 920 cm^{-1} gradually shifts to 928 cm^{-1} and a new band at 905 cm^{-1} starts to appear as the temperature rises above 220 °C. The band at 864 cm^{-1} and its shoulder at 820 cm^{-1} disappear and a broad band at 844 cm^{-1} appears as the temperature approaches 290 °C. The band at 657 cm^{-1} decreases in intensity and shifts to 681 cm^{-1}. The weak bands at 525 and 420 cm^{-1} disappear and the weak bands at 374 and 342 cm^{-1} broaden and decrease in intensity as the temperature rises to 290 °C. Major spectral changes observed in the temperature range from 220 to 240 °C are the result of the fourth dehydration where $Bi_2Mo_3O_{12}·2H_2O$ transforms to anhydrous $Bi_2Mo_3O_{12}$. The crystal structure of anhydrous $Bi_2Mo_3O_{12}$ has not been reported. However, an X-ray diffraction pattern recorded contained no measurable peaks suggesting that the powder is amorphous (data not shown).

Phase Transformations

Figure 2(B)(f) shows the representative spectral variations in the MoO_4^{2-} region from 200 to 1200 cm^{-1} for the onset of crystallization of the α-$Bi_2Mo_3O_{12}$ phase from the $Bi_2Mo_3O_{12}$ amorphous phase. The crystallization process began at 312 °C. The spectrum at 350 °C shows traces of the amorphous phase as well as the α-$Bi_2Mo_3O_{12}$ phase. The weak bands at 996, 959, 504, 374, and 289 cm^{-1} are due to the α-$Bi_2Mo_3O_{12}$ phase whereas the sharp bands at 905, 672, and 328 cm^{-1} represent the amorphous phase. The band at 928 cm^{-1} (290 °C) shifts to 905 cm^{-1} as the temperature approaches 350 °C. A further increase in temperature to 450 °C, as in Figure 2(B)(g), shows sharp bands at 996, 959, 899, 824, 669, 504 370, 340, 324, and 289 cm^{-1} characteristic of the α-$Bi_2Mo_3O_{12}$ phase. A major shift in the band at 905 cm^{-1} to 899 cm^{-1} was observed. There were no further spectral changes up to 600 °C indicating a complete transformation into the pure α-$Bi_2Mo_3O_{12}$ phase. The crystal structure of the α-$Bi_2Mo_3O_{12}$ phase (scheelite structure) has been extensively studied and reported to be monoclinic (trigonal-bipyramidal or distorted tetrahedral) with space group $P2_1/c$ and unit cell parameters a = 7.685, b = 11.491, c = 11.929 Å with characteristic edge β = 115.40°.[33] The crystal structure, reported by Cesari et

al.,[34] shows that the α-$Bi_2Mo_3O_{12}$ phase consists of two kinds of twin tetrahedra $\alpha_1\alpha_1$ and $\alpha_2\alpha_3$, one of which ($\alpha_1\alpha_1$) contains a center of symmetry; α_1 and α_2 have Bi ions adjacent to the tetrahedra, while there is a Bi ion vacancy in the α_3 tetrahedron. In all cases, there are three different and distorted tetrahedra, resulting in complicated absorption bands.

Intensity Variation

The thermo-Raman intensity (TRI) and the derivative of the thermo-Raman intensity (DTRI) of the water bands in the range from 3100 to 3700 cm^{-1} from 25 to 300 °C were plotted as shown in Figure 3(a) and (b), respectively. Based on the TGA information, the loss in intensity is equated with loss of five molecules of water. Slopes in the TRI thermogram indicate loss of water and plateaus imply intermediate formation. The TRI thermogram shows four slopes and four plateaus corresponding to four steps of dehydration. The temperature range, percentage reduction in intensity (between two intermediates), equivalent number of molecules of water lost and dip observed in the DTRI during each step of dehydration are tabulated in Table 2. The entire dehydration process extended up to 290 °C and no further decrease in intensity was observed, indicating completion of the dehydration. The slight temperature variations in the starting and end point of each of the dehydration steps in the TRS and TGA can be attributed to the different physical properties monitored by these techniques. TRS monitors the surface of the sample whilst TGA monitors the bulk. However, the end point of the completion of the dehydration process was the same for both techniques.

Band Shift

Figure 4 shows the shifts of the bands at 920 and 866 cm^{-1} plotted as a function of temperature (from 25 to 600 °C). No noticeable shift in the band at 866 cm^{-1} was observed until it gradually disappeared during the fourth step of dehydration. A similar trend was observed for the characteristic band at 920 cm^{-1}, although it showed a gradual shift to 928 cm^{-1} during the fourth step of dehydration. This clearly indicates that a major structural transformation occurs during the fourth dehydration, where two water molecules (water of constitution) are lost, distorting the structure and the environment around the MoO_4^{2-} ions. Furthermore, a drastic shift of the band from 928 to 905 cm^{-1} was observed around 310 °C during the onset of crystallization towards the formation of α-$Bi_2Mo_3O_{12}$ phase. As the temperature rose above 310 °C the band shifted gradually to 899 cm^{-1} after which no further shift was noted marking completion of transformation into the α-$Bi_2Mo_3O_{12}$ phase.

Characterization of the α-$Bi_2Mo_3O_{12}$ Phase

Morphological characteristics depend on the rate of heating and calcination time. The particle size is important and

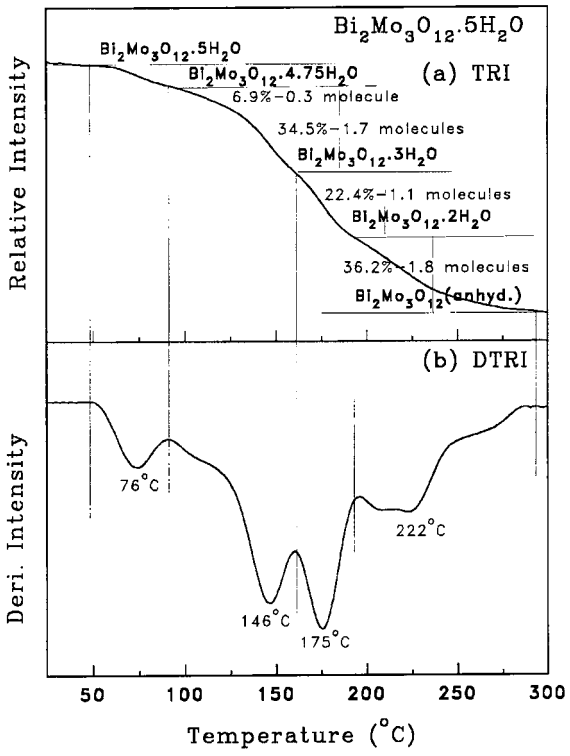

Figure 3. (a) Thermo-Raman intensity (TRI) thermogram and (b) differential thermo-Raman intensity (DTRI) thermogram for the stretching bands of H_2O during dehydration of $Bi_2Mo_3O_{12}\cdot 5H_2O$ in the temperature range from 25 to 300 °C

governs the activity and selectivity of bismuth molybdates, which must provide sufficient lattice oxide ions during catalytic redox cycles.[35]

Fourier Transform Infrared Spectroscopy

Figure 5 shows the FT-IR spectra of as-synthesized $Bi_2Mo_3O_{12}\cdot 5H_2O$ and the α-$Bi_2Mo_3O_{12}$ phase (sample collected at 450 °C). The IR spectra and the bands of the α-$Bi_2Mo_3O_{12}$ phase are in agreement with those observed by Matsuura et al.[18] The major difference observed was the disappearance of water bands and the bands at 1189 and 1879 cm^{-1}. In addition, a drastic decrease in intensity was noted in the spectra of the α-$Bi_2Mo_3O_{12}$ phase with a major splitting around 900 cm^{-1}.

X-ray Diffraction (XRD)

The XRD patterns of $Bi_2Mo_3O_{12}\cdot 5H_2O$ and the α-$Bi_2Mo_3O_{12}$ phase are shown in Figure 6. The XRD pattern of the amorphous phase contains no diffraction peaks (data not shown). The crystalline nature of $Bi_2Mo_3O_{12}\cdot 5H_2O$ and the α-$Bi_2Mo_3O_{12}$ phase is demonstrated by the presence of distinct diffraction peaks. However, notable changes in the diffraction patterns between the two crystalline forms was observed which agrees with the considerable spectral changes observed in our thermo-Raman study. The diffraction pattern of pure α-$Bi_2Mo_3O_{12}$ is in close agreement with that reported by Li and Cheng.[5] Measurement of the XRD

Table 2. TRI and DTRI data obtained during dehydration of $Bi_2Mo_3O_{12}·5H_2O$

Dehydration	Temperature. range [°C]	Intensity drop (% of H_2O)	H_2O molecules [equiv.]	DTRI endotherm [°C]
First step ($Bi_2Mo_3O_{12}·5H_2O$ to $Bi_2Mo_3O_{12}·4.75H_2O$)	50−95	6.9	0.3	76
Second step ($Bi_2Mo_3O_{12}·4.75H_2O$ to $Bi_2Mo_3O_{12}·3H_2O$)	100−160	34.5	1.7	146
Third step ($Bi_2Mo_3O_{12}·3H_2O$ to $Bi_2Mo_3O_{12}·2H_2O$)	165−190	22.4	1.1	175
Fourth step ($Bi_2Mo_3O_{12}·2H_2O$ to anhyd. $Bi_2Mo_3O_{12}$)	190−290	36.2	1.8	222

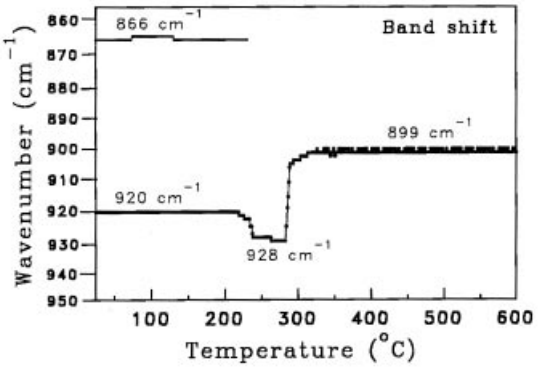

Figure 4. Band-shift measurements for the bands at 920 and 866 cm^{-1} of $Bi_2Mo_3O_{12}·5H_2O$ observed in the temperature range from 25 to 600 °C

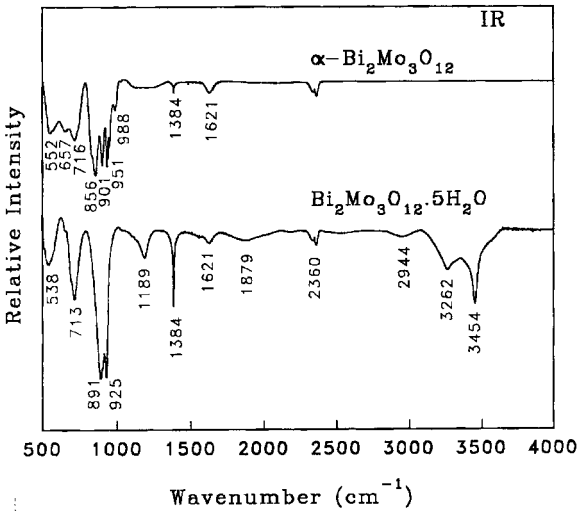

Figure 5. Fourier transform infrared spectra of as-synthesized $Bi_2Mo_3O_{12}·5H_2O$ and α-$Bi_2Mo_3O_{12}$ in the range from 500 to 4000 cm^{-1}

patterns of the intermediate hydrated species should be of interest for a better comparison with the data obtained from thermo-Raman spectroscopy. Ideally, an in situ measurement of the temperature dependence of the XRD spectrum over the temperature range of interest is required to obtain accurate data.

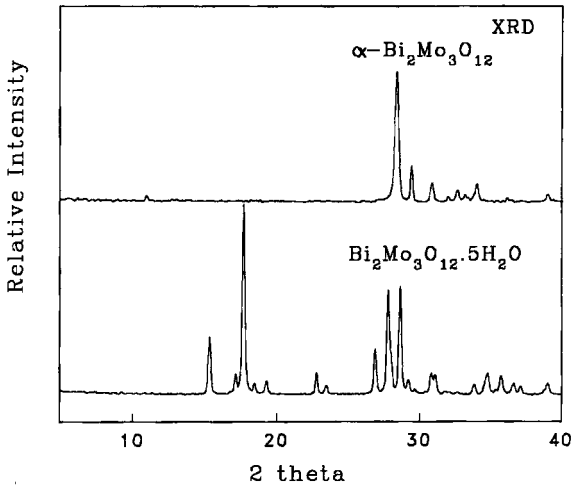

Figure 6. XRD pattern of as-synthesized $Bi_2Mo_3O_{12}·5H_2O$ and α-$Bi_2Mo_3O_{12}$ (heated to 450 °C)

Time of Flight Secondary Ionization Mass Spectrometry (TOF SIMS)

The positive ion static TOF-SIMS spectrum of the α-$Bi_2Mo_3O_{12}$ phase was also recorded and is presented in Figure 7. The observed spectral pattern and the $Bi_3O_4^+/Bi^+$ ratio of 0.0004 are in close agreement with that previously reported for the α-$Bi_2Mo_3O_{12}$ phase.[16] Considering the sensitivity of TOF-SIMS, the phase purity of α-$Bi_2Mo_3O_{12}$ can be confirmed. However, the peaks at m/z = 487 and 565 reported by Weng et al.[16] were not observed.

Electron Microscopic Study and EDS Analysis

Electron microscopy is extensively used for structural, chemical (composition), and morphological studies (grain size, crystallinity, and phase identification). Figure 8(a) shows a TEM image of the α-$Bi_2Mo_3O_{12}$ phase obtained after controlled heating to 450 °C at a rate of 5 °C·min^{-1}. The distribution of the particle size was in the range of several hundreds of nanometers (avg. 200 nm) as observed from the particle size distribution profile deduced from TEM images [Figure 8,(b)]. However, in most of the earlier reports where the calcination step probably involved fast heating rates, the particle size was reported to be in the

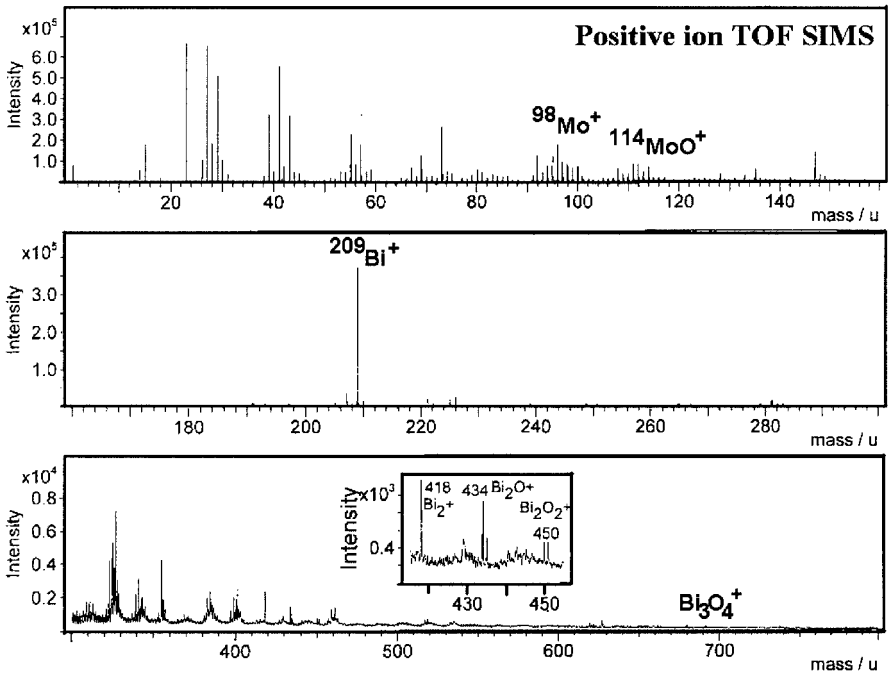

Figure 7. Positive ion TOF-SIMS spectra of α-$Bi_2Mo_3O_{12}$ (heated to 450 °C)

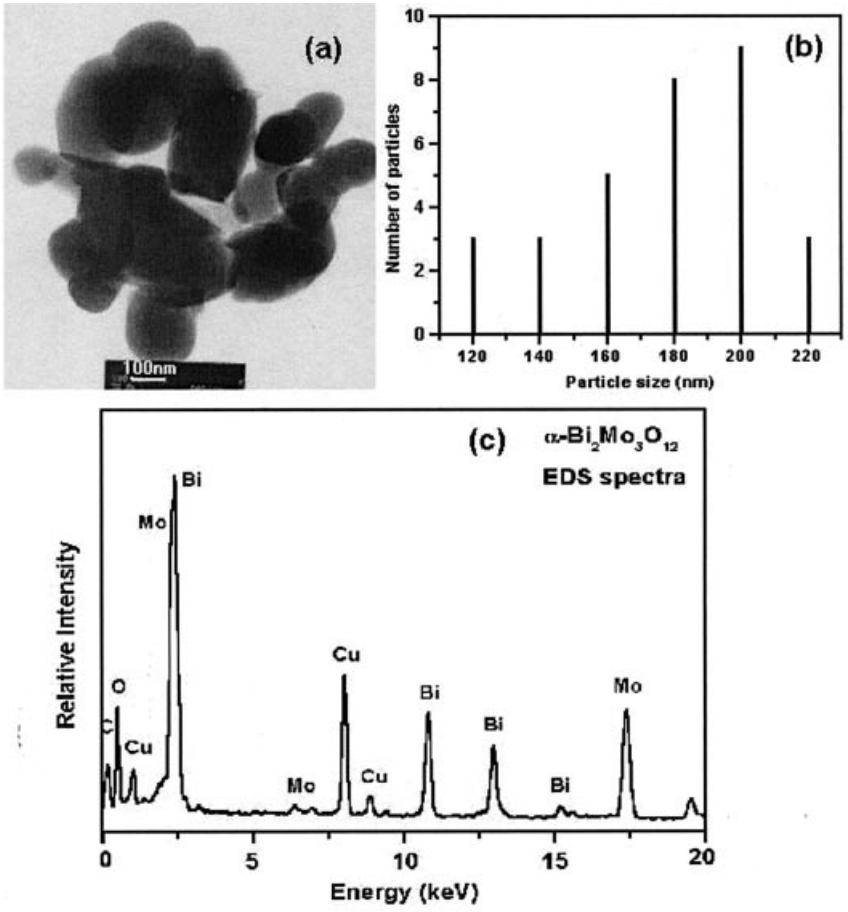

Figure 8. Morphological and compositional characterization of α-$Bi_2Mo_3O_{12}$ (heated to 450 °C): (a) TEM image indicating the particle size and surface characteristics; (b) particle size distribution profile; (c) EDS spectra showing the composition of the α-$Bi_2Mo_3O_{12}$ formed (atomic ratio Bi/Mo ≈ 2:3)

micrometer range (100−400 μm).[36] EDS is useful for quantitative analysis. EDS measurements were carried out on $Bi_2Mo_3O_{12}·5H_2O$, α-$Bi_2Mo_3O_{12}$ (heated at 450 °C), and α-$Bi_2Mo_3O_{12}$ (heated at 550 °C). The presence of bismuth, molybdenum, and oxygen was examined and a representative EDS spectrum of α-$Bi_2Mo_3O_{12}$ (heated at 550 °C) is shown in Figure 8(c). The bismuth and molybdenum contents, and the Bi/Mo ratios in all the samples were identical. The atomic ratio of Bi/Mo was observed to be 43:57 which is in close agreement with the molar ratios of Bi_2O_3/$Na_2MoO_4·2H_2O$ in the starting solution.

According to AFM, XRD, and XPS experiments carried out by Yanina and Smith,[37] a loss of Mo was observed on heating to temperatures higher than 500 °C in dry air or air with 2.3% H_2O due to volatilization. This resulted in precipitation of traces of γ-Bi_2MoO_6 and β-$Bi_2Mo_2O_9$ on the surface of the α-$Bi_2Mo_3O_{12}$ catalyst. However, no such changes were observed in our experiments even though the heating was performed in the presence of air. This might be due to the slow and controlled heating rate used in our experiment. Additionally, TOF-SIMS data also support the presence of the α-$Bi_2Mo_3O_{12}$ phase. This provides evidence for the formation of the pure form of the α-$Bi_2Mo_3O_{12}$ catalyst under a controlled heating rate in the presence of air. In addition, the particle size observed from TEM images lies in the hundreds of nanometers range, suggesting that the controlled heating rate is also important in governing the particle size of the catalyst.

Conclusion

A systematic study of the dehydration and phase-transformation processes of $Bi_2Mo_3O_{12}·5H_2O$ was carried out using thermo-Raman spectroscopy in the temperature range from 25 to 600 °C. Three different hydrated species, $Bi_2Mo_3O_{12}·4.75H_2O$, $Bi_2Mo_3O_{12}·3H_2O$, $Bi_2Mo_3O_{12}·2H_2O$, and anhydrous $Bi_2Mo_3O_{12}$ were observed as intermediates, based on the spectral variations observed in the H_2O and MoO_4^{2-} absorption regions during temperature increments of 1 °C. Characteristic Raman spectra of these hydrated species have been reported for the first time. The TRI thermogram for the H_2O bands supported the results revealing four dehydration steps with a proportionate loss of water in each step. The DTRI thermogram was also in harmony with the TRI and TGA data. The phase transformation of anhydrous $Bi_2Mo_3O_{12}$ to the α-$Bi_2Mo_3O_{12}$ phase was also observed and characterized by other techniques. Slow and controlled heating resulted in the α-$Bi_2Mo_3O_{12}$ phase without precipitating γ-Bi_2MoO_6 and β-$Bi_2Mo_2O_9$ phases and the particle size thus obtained was in the range of a few hundreds of nanometers as observed from the morphological characterization. The characterization of the α-$Bi_2Mo_3O_{12}$ phase by XRD, EDS, and FTIR for phase purity was further supported by TOF-SIMS analysis. The fact that the thermo-Raman spectroscopy setup could detect all the dehydration steps involved and also the transformation to the α-$Bi_2Mo_3O_{12}$ phase indicates its sensitivity and potential future applications in monitoring catalyst formation if a commercial instrument can be developed.

Experimental Section

Sample Preparation: Bi_2O_3 (Aldrich Chem., WI, USA) and $Na_2MoO_4·2H_2O$ (Riedel−de Haën, Seelze, Germany) were used as received without further purification. Bi_2O_3 and $Na_2MoO_4·2H_2O$ (1:3 molar ratio) were dissolved in 1 M nitric acid and stirred vigorously at 60 °C until a slurry was obtained. This slurry was cooled, filtered, and the residue washed thoroughly with distilled water until the washings reached pH = 6. The sample was dried at room temperature to ensure the retention of water of hydration. This sample was lightly ground prior to analysis.

Thermo-Raman Study: The Raman spectra were obtained using laser excitation at a wavelength of 514.5 nm (50 mW) from an argon ion laser (Coherent, Innova 100-15). A filter was used to remove the plasma lines. The scattered light was collected at right angles, dispersed by a single spectrometer (Spex, 0.5 m) with a resolution of 2 cm^{-1} and detected by a CCD camera (Princeton Instruments, 1024 × 1024 pixels). A notch filter was set in front of the spectrometer to remove the Rayleigh scattered light. The sample was placed in a sample holder and mounted on the thermocouple in a homemade oven in stationary air. The temperature of the oven was programmed to increase from 25 to 600 °C at a rate of 5 °C min^{-1}. Thermo-Raman spectra were collected continuously during heating without disturbing the sample. The exposure time of the CCD was set such that the temperature range covered by each spectrum was 1 °C. Overall, 575 spectra were collected and their reproducibility checked in the spectral range from 200 to 1400 cm^{-1} for MoO_4^{2-} whilst 275 spectra in the range from 2900 to 3900 cm^{-1} were collected for H_2O. A BASIC computer program was written to systematically determine the intensity variation for TRI thermogram and the band-shift measurements.

Characterization: A thermogravimetric analyzer (Perkin−Elmer TGA6) was used to record the thermogram in the temperature range from 25 to 600 °C with a heating rate of 5 °C·min^{-1} in a flow of air at 20 mL·min^{-1}. The DSC thermogram of the same sample was recorded with a Setaram DSC131 in a crimped aluminum crucible in the temperature range from 25 to 550 °C with a heating rate of 5 °C·min^{-1} in a flow of air at 30 mL·min^{-1}. Fourier transform infrared spectroscopy was carried out with a Bomem Hartmann & Braun (MB-series) spectrometer. The X-ray diffraction patterns of the product were measured with a Material Analysis and Characterization (MAC) advanced powder X-ray diffractometer using Cu-$K_{\alpha 1}$ radiation (1.54056 Å). Positive TOF SIMS (ION-TOF) measurements were performed using pulsed Ga^+ ions (15 keV) and a post-acceleration of 10 kV. The analysis area of 100 μm × 100 μm with data acquisition time of 200 s was used for static TOF-SIMS conditions. The best resolution obtained was $M/\Delta M \approx 8000$. The powders were pressed on to the carbon tape supported on a clean Si wafer. Excess particles were removed by blowing with compressed air such that the layer thickness was minimal. The particle morphology was studied by transmission electron microscopy (TEM) (Philips, Tecnai 20) working at a 200 kV accelerating voltage. A drop of sample suspension, which had been previously dispersed in methanol by ultrasonication, was placed on the microgrid and dried before microscopy study. The elemental composition of the material was analyzed by energy-dispersive X-ray analysis (EDS) (Philips, Tecnai 20).

Acknowledgments

This work was supported by the National Science Council of the Republic of China (NSC91-2113-M007-056).

[1] [1a] R. K. Grasselli, *Handbook of Heterogeneous Catalysis* (Eds.: G. Ertl, H. Knözinger, J. Weitkamp), Wiley-VCH, Weinheim, **1997**, vol. 5. [1b]T. D. Snyder, G. C. Hill, Jr., *Catal. Rev. Sci. Eng.* **1989**, *31*, 43−95. [1c] R. K. Grasselli, J. D. Burrington, J. F. Brazdil, *Faraday Discuss. Chem. Soc.* **1982**, *72*, 203−223.
[2] C. N. Satterfield, *Heterogeneous Catalysis in Industrial Practice*, McGraw Hill, New York, **1991**.
[3] [3a] J. L. Callahan, R. K. Grasselli, E. C. Milberger, H. A. Strecker, *Ind. Eng. Chem. Prod. Res. Develop.* **1970**, *9*, 134−142. [3b] J. M. M. Millet, H. Ponceblanc, G. Coudurier, J. M. Herrmann, J. C. Vedrine, *J. Catal.* **1993**, *142*, 381−391.
[4] [4a] B. C. Gates, J. R. Katzer, G. C. A. Schuit, *Chemistry of Catalytic Processes*, McGraw Hill, New York, United States **1979**, chapter 4. [4b] G. W. Keulks, L. D. Krenzke, T. M. Notermann, *Adv. Catal.* **1978**, *27*, 183−225. [4c] R. K. Grasselli, J. D. Burrington, *Adv. Catal.* **1981**, *30*, 133−163. [4d] Y. Moro-Oka, W. Ueda, *Adv. Catal.* **1994**, *40*, 233−273. [4e] M. M. Bettahar, G. Costentin, L. Savary, J. C. Lavalley, *Appl. Catal. A.* **1996**, *145*, 1−48.
[5] K. T. Li, W. D. Cheng, *Appl. Catal. A: Gen.* **1996**, *142*, 315−326.
[6] R. N. Vannier, F. Abraham, G. Nowogrocki, G. Mairesse, *J. Solid State Chem.* **1999**, *142*, 294−304.
[7] V. Marinova, M. Veleva, *Opt. Mater.* **2002**, *19*, 329−333.
[8] D. K. Biegelsen, T. Chen, J. C. Zesch, *J. Appl. Phys.* **1975**, *46*, 941−942.
[9] K. Y. Kang, P. H. Her, M. S. Jang, H. K. Kim, H. L. Park, D. Finotello, M. H. W. Chan, *Solid State Commun.* **1988**, *67*, 723−724.
[10] T. Sekiya, A. Tsuzuki, Y. Torii, *Mater. Res. Bull.* **1985**, *21*, 601−608.
[11] N. Hykaway, W. M. Sears, R. F. Frindt, S. R. Morrison, *Sens. Actuators* **1988**, *15*, 105−118.
[12] F. D. Hardcastle, I. E. Wachs, *J. Phys. Chem.* **1991**, *95*, 10763−10772.
[13] M. R. Antonio, R. G. Teller, D. R. Sandstrom, M. Mehicic, J. F. Brazdil, *J. Phys. Chem.* **1988**, *92*, 2939−2944.
[14] [14a] A. F. Van den Elzen, G. D. Rieck, *Mater. Res. Bull.* **1975**, *10*, 1163−1168. [14b] Z. Wuzong, D. A. Jefferson, M. Alario-Franco, J. M. Thomas, *J. Phys. Chem.* **1987**, *91*, 512−514.
[15] F. Theobald, A. Laarif, A. W. Hewat, *Mater. Res. Bull.* **1985**, *20*, 653−665.
[16] L. T. Weng, P. Bertrand, O. Tirions, M. Devillers, *Appl. Surf. Sci.* **1996**, *99*, 185−196.
[17] D. J. Buttrey, D. A. Jefferson, J. M. Thomas, *Philos. Mag. A* **1986**, *53*, 897−906.
[18] I. Matsuura, R. Schut, K. Hirakawa, *J. Catal.* **1980**, *63*, 152−166.
[19] J. M. Stencel, *Raman Spectroscopy for Catalysis*, Van Nostrand Reinhold, New York, **1990**, vol. 2.
[20] T. Ono, N. Ogata, R. L. Kuczkowski, *J. Catal.* **1998**, *175*, 185−193.
[21] [21a] K. Nakamoto, *Infrared and Raman Spectra of Inorganic and Coordination Compounds*, 3rd ed, Wiley, New York, **1978**. [21b] L. Dixit, D. L. Gerrard, H. J. Bowley, *Appl. Spectrosc. Rev.* **1986**, *22*, 189−249.
[22] [22a] Ph. A. Batist, J. F. H. Bouwens, G. C. A. Schuits, *J. Catal.* **1972**, *25*, 1−11. [22b] B. Grzybowska, J. Haber, J. Komorek, *J. Catal.* **1972**, *25*, 25−32.
[23] J. D. Grunwaldt, M. D. Wildberger, T. Mallat, A. Baiker, *J. Catal.* **1998**, *177*, 53−59.
[24] I. VanDriessche, R. Mouton, S. Hoste, *Mater. Res. Bull.* **1996**, *31*, 979−992.
[25] F. Trifiro, H. Hoser, R. D. Scarle, *J. Catal.* **1972**, *25*, 12−24.
[26] D. J. Buttrey, T. Vogt, B. D. White, *J. Solid State Chem.* **2000**, *155*, 206−215.
[27] E. Godard, E. M. Gaigneaux, P. Ruiz, B. Delmon, *Catal. Today* **2000**, *61*, 279−285.
[28] W. W. Wendlandt, *Thermal Analysis*, 3rd ed., Wiley, New York, **1986**.
[29] [29a] H. Chang, P. J. Huang, *Anal. Chem.* **1997**, *69*, 1485−1491. [29b] A. Ghule, R. Murugan, H. Chang, *Inorg. Chem.* **2001**, *40*, 5917−5923. [29c] A. Ghule, R. Murugan, H. Chang, *Thermochim. Acta* **2001**, *371*, 127−135.
[30] Y. Murakami, H. Imai, *J. Mater. Sci. Lett.* **1990**, *10*, 107−108.
[31] S. Yinjie, Z. Aimin, *J. Radioanal. Nucl. Chem.* **1998**, *231*, 17−20.
[32] C. J. Serna, M. Ocana, J. E. Iglesias, *J. Chem. Phys.* **1987**, *C20*, 473−484.
[33] [33a] A. F. Van den Elzen, G. D. Rieck, *Acta Crystallogr., Sect. B* **1973**, *29*, 2433−2436. [33b] S. Miyazawa, A. Kawana, H. Koizumi, H. Iwasaki, *Mater. Res. Bull.* **1974**, *9*, 41−52.
[34] M. Cesari, G. Perego, A. Zazzetta, G. Manara, B. Notari, *J. Inorg. Nucl. Chem.* **1971**, *33*, 3595−3597.
[35] [35a] Y. H. Han, W. Ueda, Y. Moro-Oka, *Appl. Catal. A* **1999**, *176*, 11−16. [35b] N. Arora, G. Deo, I. E. Wachs, A. M. Hirt, *J. Catal.* **1996**, *159*, 1−13.
[36] P. Boutry, R. Montarnal, J. Wrzyszcz, *J. Catal.* **1969**, *13*, 75−82.
[37] S. V. Yanina, R. L. Smith, *J. Catal.* **2003**, *213*, 151−162.

Received August 28, 2003
Early View Article
Published Online March 5, 2004

